ISSN 0006-2979, Biochemistry (Moscow), 2023, Vol. 88, No. 10, pp. 1580-1595 © Pleiades Publishing, Ltd., 2023.
Published in Russian in Biokhimiya, 2023, Vol. 88, No. 10, pp. 1908-1925.

Femtosecond Dynamics of Excited States of Chlorophyll Tetramer in Water-Soluble Chlorophyll-Binding Protein BoWSCP

Dmitry A. Cherepanov[1,2,a]*, Konstantin V. Neverov[3,4], Yuriy N. Obukhov[3], Yulia V. Maleeva[4], Feodor E. Gostev[1], Ivan V. Shelaev[1,2], Arseny V. Aybush[1], Michail S. Kritsky[3], and Victor A. Nadtochenko[1,5,b]*

[1] *Semenov Federal Research Center for Chemical Physics, Russian Academy of Sciences, 119991 Moscow, Russia*

[2] *Belozersky Research Institute of Physical and Chemical Biology, Lomonosov Moscow State University, 119992 Moscow, Russia*

[3] *Bach Institute of Biochemistry, Federal Research Center "Fundamentals of Biotechnology" of the Russian Academy of Sciences, 119071 Moscow, Russia*

[4] *Faculty of Biology, Lomonosov Moscow State University, 119991 Moscow, Russia*

[5] *Faculty of Chemistry, Lomonosov Moscow State University, 119991 Moscow, Russia*

[a] *e-mail: tscherepanov@gmail.com*

[b] *e-mail: nadtochenko@gmail.com*

Received June 22, 2023
Revised September 22, 2023
Accepted September 22, 2023

Abstract—The paper reports on the absorption dynamics of chlorophyll *a* in a symmetric tetrameric complex of the water-soluble chlorophyll-binding protein BoWSCP. It was measured by a broadband femtosecond laser pump-probe spectroscopy within the range from 400 to 750 nm and with a time resolution of 20 fs-200 ps. When BoWSCP was excited in the region of the Soret band at a wavelength of 430 nm, nonradiative intramolecular conversion $S_3 \rightarrow S_1$ was observed with a characteristic time of 83 ± 9 fs. When the complex was excited in the region of the Q_y band at 670 nm, relaxation transition between two excitonic states of the chlorophyll dimer was observed in the range of 105 ± 10 fs. Absorption spectra of the excited singlet states S_1 and S_3 of chlorophyll *a* were obtained. The delocalization of the excited state between exciton-coupled Chl molecules in BoWSCP tetramer changed in time and depended on the excitation energy. When BoWSCP is excited in the Soret band region, an ultrafast photochemical reaction is observed. This could result from the reduction of tryptophan in the vicinity of chlorophyll.

DOI: 10.1134/S0006297923100139

Keywords: chlorophyll *a*, WSCP proteins, femtosecond laser spectroscopy, excited state spectrum, exciton dynamics, intramolecular conversion

INTRODUCTION

Analysis of the photochemical reactions of energy transfer and charge separation in photosynthetic pigment–protein complexes is challenging due to their complicated molecular organization and a large number of exciton-coupled chlorophyll (Chl) molecules. Furthermore, interpretating the absorption dynamics of photosynthetic complexes registered by femtosecond laser spectroscopy is a challenging methodological issue [1, 2]. Water-soluble chlorophyll-binding proteins (WSCP) from higher plants represent an ideal model system to study the mechanism of photochemical reactions [3-6]. These proteins are water-soluble, photostable and thermally stable, and can be effectively modified and produced through genetic and protein engineering methods. In a plant cell these proteins are

Abbreviations: BoWSCP, water-soluble chlorophyll-binding protein (WSCP) from *Brassica oleracea* var. *botrytis*; Chl, chlorophyll.

* To whom correspondence should be addressed.

located outside the thylakoid membranes of chloroplasts and do not contribute to photosynthesis. Their physiological functions are thought to be related to the activity of the cells anti-stress systems [4, 7, 8].

Compared to the photosynthetic pigment–protein complexes, WSCP protein structure is relatively simple. WSCP holoforms are water-soluble homotetramers with a molecular weight of 69-80 kDa. Each complex contains up to four noncovalently bound Chl molecules. Depending on homology of the primary apoprotein structure, WSCP proteins are subdivided into classes I and II, and the latter has subclasses IIa and IIb by different affinity of apoproteins for Chl *a* and *b* [6, 9]. It was shown that upon photoexcitation of Chl in WSCP, energy migration occurs both within the dimer and between dimer pairs [10, 11]. This makes class II WSCP a promising model for studying the mechanisms of pigment–pigment and pigment–protein interactions, which will enable research into the mechanisms of excitation energy transfer between pigments [12-14] and interaction of the excited pigments with surrounding proteins [15-17].

In this paper, a broadband femtosecond laser pump-probe spectroscopy was used for studying photochemical processes in a symmetric tetrameric complex of the water-soluble chlorophyll-binding protein BoWSCP (subclass IIa) from *Brassica oleracea* var. *botrytis*, which mainly binds Chl *a*, i.e., its pigment composition can be considered as almost homogeneous [5]. The tetrameric Chl complex in BoWSCP is in the form of two dimers, and the angle between porphyrine nuclei of pigments in the dimer is about 30° [18]. Taken together, the two dimers in a holoprotein macromolecule form a non-covalent tetrameric structure, where Chl dimer pairs are connected by phytol tails [19]. The exciton interaction energy of monomers in the dimer is approximately 100 cm^{-1}, while the interaction between dimers is an order of magnitude weaker [13, 20]. It has recently been shown that Chl forming part of this structure manifests photocatalytic activity in redox processes [21].

This work aims to quantitatively analyse the processes of nonradiative intramolecular conversion from the third excited state to the lowest one, and electronic transitions between exciton substates of the Q_y band of the Chl *a* tetramer when BoWSCP is excited in the region of the Soret band and the Q_y band, respectively. Spectral characteristics are considered, which allow the determination of the degree of exciton delocalization between Chl molecules in the BoWSCP tetrameric complex and the detection of electron transfer reactions involving excited Chl molecules.

MATERIALS AND METHODS

BoWSCP apoprotein preparations were obtained by expression of genes encoding this protein incorporated in a plasmid, by which cells of *Escherichia coli* BL21(DE3) producer strain were transformed, in accordance with the protocol [5, 6, 22]. Due to six histidine residues (6xHis) on N-terminal domains of apoproteins, their preparations were purified using affinity chromatography on a Ni-agarose column with a subsequent preparation dialysis. Preparation purity was tested using denaturing polyacrylamide gel electrophoresis [5, 6]. Self-assembly of BoWSCP holoforms was performed *in vitro* by joint incubation of apoproteins and isolated thylakoid membranes of spinach [4-6, 8, 22]. Taking into account high thermal stability of WSCP protein tetramers, the obtained holoform preparations were heated (95°C, 10 min) to remove unnecessary proteins. The final purification of BoWSCP was then carried out on the Ni-agarose column [1, 23]. The purified preparation was dialysed against 10 mM Tris-HCl buffer, pH 8.0. Quality of BoWSCP tetramer preparations was tested using native polyacrylamide gel electrophoresis, absorption spectroscopy, fluorescence spectroscopy and circular dichroism spectroscopy. Denaturating and native electrophoresis of proteins was carried out in Mini PROTEAN Tetra System (Bio-Rad, USA). Protein content in samples was measured using the Bradford assay [24]. The absorption spectra of the samples were registered using Cary-50 (Agilent, USA) and Shimadzu-1601PC (Shimadzu, Japan) spectrophotometers. Circular dichroism (CD) spectra were registered using Chirascan circular dichroism instrument (Applied Photophysics, USA). Signal amplitude ($\Delta\varepsilon$) was converted into units of ellipticity (θ) for circular dichroism spectra in accordance with [23].

Preparations for femtosecond spectroscopy were concentrated by centrifugation in Amicon Ultra-15 centrifugal devices with 30 or 50 kDa filters. Concentration was achieved by centrifugation of BoWSCP preparations (several times) in 10 mM Tris-HCl buffer, pH 8.0, with addition of up to 150 mM NaCl or 10% glycerine to prevent protein aggregation in the highly concentrated solution. The concentrate was diluted with the same buffer with NaCl or glycerine to obtain 1 ml of solution with $OD_{673} = 5$.

Ultrafast absorption changes $\Delta A(\lambda_i, t_m)$ were recorded by the femtosecond pump-probe laser spectroscopy in the spectral range of $400 \leqslant \lambda \leqslant 780$ nm and time delays from 20 fs to 200 ps. The experimental setup and measurement methodology were described earlier [25]. The excitation of the BowSCP was achieved by femtosecond pulses with a maximum at 430 nm (duration 40 fs, energy 20 nJ) and 670 nm (duration 16 fs, energy 15 nJ). Absorption changes were enquired by the broadband pulses at the polarization angles of 0, 54.7, and 90 degrees relative to the exciting pulse polarization. The difference absorption spectra in the range of 400-780 nm were registered using the CCD-camera (Roper Scientific SPEC-10, USA), connected to the polychro-

mator (Acton SP-300, USA). The experiments were carried out at a temperature of 6°C in a circulating optical cell 0.5 mm thick, the diameter of optical windows 0.2 mm, the optical density of the sample 10 cm^{-1}. The rate of sample circulation (9 ml/min) was high enough to avoid multiple excitations of the same sample volume. The spectra were corrected by the group delay dispersion, as previously described [26, 27]. Deconvolution of the instrumental function accounting for the coherent artifact in the region $t = 0$ was carried out according to the method proposed in the works [26, 28]. For this purpose, the absorption changes caused by nonlinear interactions of overlapping pump and probe pulses (coherent spike) were approximated by the basic gaussian function (1):

$$G(t) = 1/\sqrt{2\pi d^2}\,\exp[-½(t/d)^2], \quad (1)$$

and its derivatives in time G' and G'', where the width of the pump pulse d was determined by the absorption changes of the pure solvent [29]. The signal related to changes in the electronic states of pigments was approximated by convolution of the basic Gaussian function $G(t)$ and the step function of Hevisaid $H(t)$ (2):

$$\chi(t) = G(t)*H(t) = ½Erfc[-t/\sqrt{2\pi d^2}], \quad (2)$$

as well as convolutions of $G(t)$ and exponential functions (3):

$$\varepsilon(t,\tau_k) = G(t)*\exp(-t/\tau_k) = \\ = ½\exp[½(d/\tau_k)^2 - t/\tau_k]\,Erfc[(d/\tau_k - t/d)/\sqrt{2}]. \quad (3)$$

The amplitudes $A_k(\lambda_i)$ were determined by linear regression and the characteristic times τ_k by nonlinear minimization.

The mathematical analysis of the absorption dynamics included approximation of spectral-temporal matrices $\Delta A(\lambda_l,t_m)$ by a linear combination of n discrete exponential functions (4):

$$Q[\boldsymbol{\tau}](\lambda,t) = \sum_{k=1}^{n} D_k(\lambda)\cdot\exp(-t/\tau_k) + D_{n+1}(\lambda), \quad (4)$$

under the assumption that the characteristic times $\boldsymbol{\tau} = \{\tau_k\}$ do not depend on the probe wavelength λ and, therefore, can be considered as "global" parameters determined by nonlinear minimization of the normalized discrepancy (5):

$$R[\boldsymbol{\tau}] = (L\cdot M - n)^{-1}\sum_{l=1}^{L}\sum_{m=1}^{M}[\Delta A(\lambda_l,t_m) - \\ - Q[\boldsymbol{\tau}](\lambda_l,t_m)]^2. \quad (5)$$

The wavelength-dependent amplitudes $D_k(\lambda)$, which were calculated by the linear regression method for each exponential function k, represent decay associated spectra (DAS). When the optimal values $\{\tau_k\}$ of characteristic times are found, the standard errors of their estimation can be evaluated using the Jacobi matrix **J** (6):

$$J_{jk} = \frac{\delta Q_j[\boldsymbol{\tau}]}{\delta\tau_k}. \quad (6)$$

Here the index j runs over $L \times M$ experimental points of the spectral-temporal matrix $\Delta A(\lambda_l,t_m)$ [30]. The numerical assessment of Jacobian can be obtained by decomposing the expression $Q_j[\boldsymbol{\tau}]$ in a Taylor series of the first order (7):

$$\frac{\delta Q_j[\boldsymbol{\tau}]}{\delta\tau_k} \approx \frac{Q_j[\boldsymbol{\tau} + \Delta\boldsymbol{\tau}e_k] - Q_j[\boldsymbol{\tau} - \Delta\boldsymbol{\tau}e_k]}{2\Delta\tau_k}. \quad (7)$$

Here $\boldsymbol{\tau}$ is a set of optimal values of characteristic times $\{\tau_k\}$, e_k is the k^{th} single vector, and $\Delta\boldsymbol{\tau}$ is a small increase of $\boldsymbol{\tau}$ (the value of $0.015\boldsymbol{\tau}$ was used for a numerical assessment). Standard errors σ_k of characteristic times estimation can be obtained from the diagonal elements of the covariance matrix $C = R[\boldsymbol{\tau}]\times(\mathbf{J}^T\mathbf{J})^{-1}$ (8):

$$\sigma_k = \sqrt{C_{kk}}. \quad (8)$$

The values of σ_k are standard deviations characterizing the uncertainty of $\{\tau_k\}$ assessments. According to the Student's t-distribution, 95% reliability is obtained with the doubling of standard deviations, so the trust intervals are $\tau_k \pm 2\sigma_k$, respectively.

RESULTS

Using the method proposed by Hughes et al. [20], the pigment composition of the obtained BoWSCP holoform preparations was determined by decomposing its absorption spectrum in the Soret band region (360-500 nm) into relative contributions of Chl *a* and Chl *b* using the absorption spectra of individual pigments in 90% acetone [31]. Figure 1a shows comparison of BoWSCP absorption spectrum with the spectra of Chl *a* and Chl *b*. In the absorption spectrum of free Chl *a*, the Soret and Q_y absorption bands with peaks at approximately 430 and 663 nm have a comparable amplitude; in the spectrum of Chl *b*, these bands are located closer to each other at 458 and 645 nm, respectively, and the amplitude of the Soret band is increased, whereas that of the Q_y band is reduced in relation to the Chl *a* bands. The presence of Chl *b* in the BoWSCP spectrum is detected based on a small "arm" in the region of 470 nm, while absorption in the interval of 380-430 nm is related mainly to Chl *a*. Comparison of the spectra of BoWSCP and free Chl *a* shows a significant effect of surrounding protein in the region of 360-450 nm. Firstly, Chl *a* bands are shifted to the red by ~8 nm. Secondly, the intensities of the two main transitions of Chl *a* in the Soret region (the B_x band with the peak at 430 nm corresponds

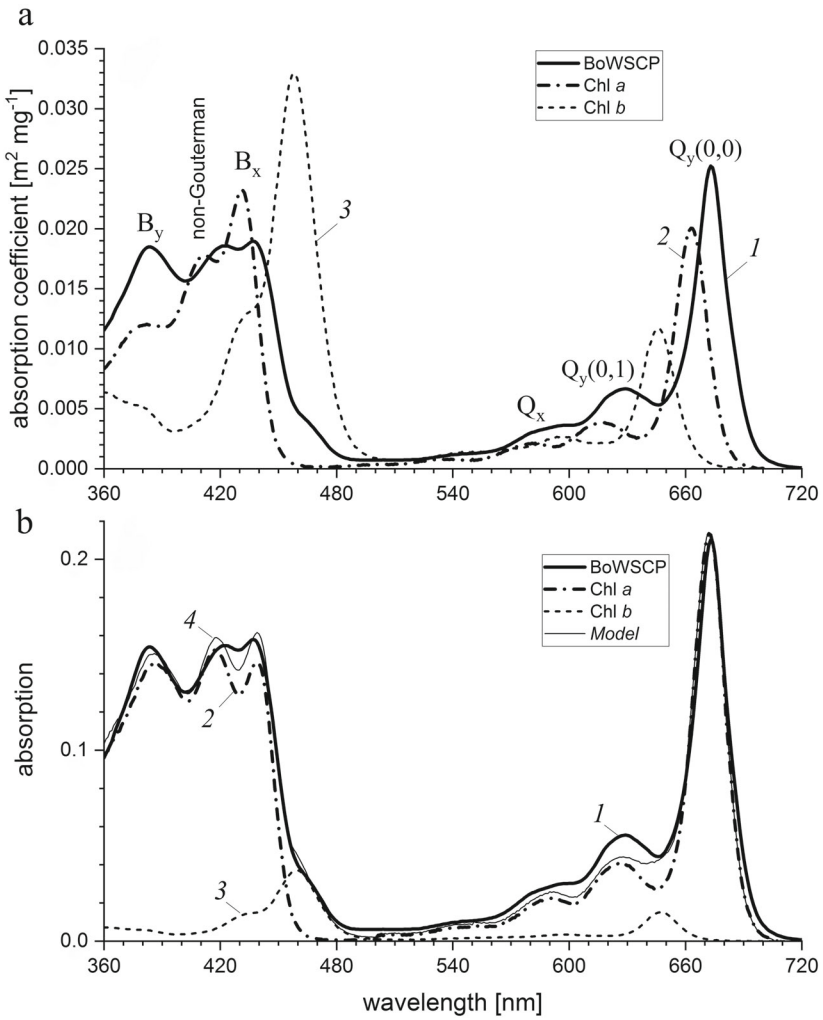

Fig. 1. Determination of the contributions of Chl *a* and Chl *b* to the absorption spectrum of BoWSCP. a) Comparison of the absorption spectrum of BoWSCP holoform in the buffer solution (*1*) with the spectra of Chl *a* (*2*) and Chl *b* (*3*) in 90% acetone (based on the open spectral database [31]). b) Modelling of BoWSCP spectrum (*1*) using Chl *a* (*2*) and Chl *b* (*3*) spectra modified in accordance with the equation (9). In the region of 500-720 nm, the amplitude of Chl *a* spectrum is increased by 15%. Relative contributions of Chl *a* and Chl *b* to the model spectrum (*4*) are 89% and 11%, respectively.

to the $S_0 \rightarrow S_3$ transition, and the B_y band with the peak at 380 nm corresponds to the $S_0 \rightarrow S_4$ transition [32]) are changed significantly in favour of the band with the peak at ~380 nm. The electronic structure of the absorption spectrum of Chl *a* in the Soret region cannot be described properly by the Gouterman four-orbital model [33], because there are non-Gouterman states between the excited B_x and B_y states, mixed with vibronic substates of the B_x band. Consequently, energy and dipole power of these states depend on dielectric surrounding of the pigment [32, 34, 35].

As follows from Fig. 1a, the relative probability of $S_0 \rightarrow S_3$ transition of Chl *a* in BoWSCP is reduced, while the probability of $S_0 \rightarrow S_4$ transition is increased compared to the properties of free Chl *a* in solution. For this reason, the BoWSCP absorption spectrum was modelled by the empirical expression representing a sum of modified absorption spectra of Chl *a* and Chl *b*, and taking into account the redistribution of Chl *a* bands intensity in the region of 360-500 nm:

$$A(\lambda) = \alpha \cdot A_{Chla}(\lambda - \delta_a) \cdot [1 - \gamma \cdot \tanh((\lambda - \lambda_a/\Delta)] + \\ + \beta \cdot A_{Chlb}(\lambda - \delta_b). \quad (9)$$

Here, α and β are the relative fractions of Chl *a* and Chl *b* in the BoWSCP tetramer, A_{Chla} and A_{Chlb} are the spectra of Chl *a* and Chl *b* in 90% acetone, δ_a and δ_b show how the spectra of Chl *a* and Chl *b* in BoWSCP are shifted relative to their spectra in the solution. The empirical function $\gamma \cdot \tanh((\lambda - \lambda_a)/\Delta)$ describes changes in the ratio of the B_x and B_y bands of Chl *a* intensities in the spectral interval centered at the wavelength λ_a and the width Δ. Values of these parameters determined by non-linear minimization amounted to: $\alpha = 89.2\%$; $\beta = 10.8\%$; $\delta_a = 9.2$ nm; $\delta_b = 1.4$ nm; $\gamma = 0.67$; $\lambda_a = 413$ nm; $\Delta = 50$ nm; the model spectrum

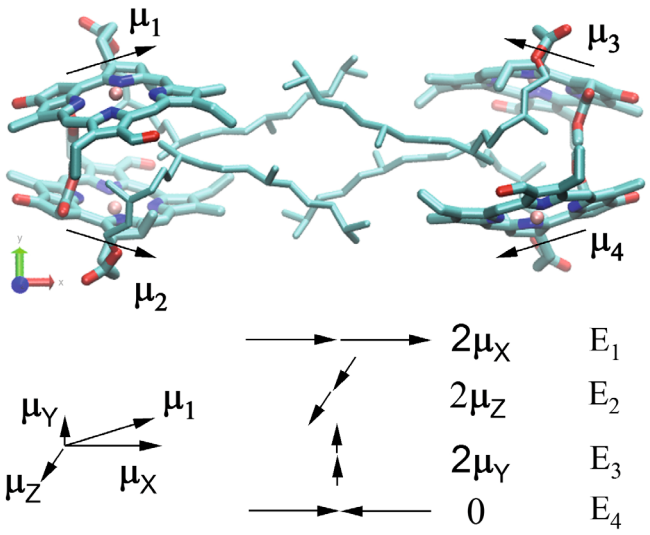

Fig. 2. Location of chlorophyll molecules in the BoWSCP tetrameric complex according to the X-ray crystallographic structure PDB ID: 6s2z [18], where Chl *b* is replaced by Chl *a*. Arrows show the directions of vectors μ_k (k = 1,...,4) characterizing the $S_0 \rightarrow S_1$ transition dipole moments of four Chl monomers, and dipole moments of four exciton states E_n of the tetrameric complex.

is shown in Fig. 1b by a thin solid line. Relative contributions of Chl *a* and Chl *b* were equal to 89% and 11%, respectively. The ratio between Chl *a*/*b* pigments of 8 : 1 corresponds to the range of values 6-10 : 1 obtained in various papers for BoWSCP native protein [3].

Absorption of BoWSCP in the Q_y band region (660-700 nm) is related primarily to Chl *a*, while the Chl *b* contribution is negligible in this interval (Fig. 1b). The BoWSCP spectral properties are adjusted by the molecular structure of the pigment–protein complex: four identical subunits form a tetramer in which three orthogonal axes of rotational symmetry $C_2(X)$ $C_2(Y)$ $C_2(Z)$ define the coordinate system XYZ [18]. Four chlorophyll molecules in the hydrophobic locus form a double dimer: interactions between dimers are much weaker than interactions between monomers within a dimer (Fig. 2).

The effect of exciton interaction between Chl molecules within the dimer predominates in the region of 660-700 nm, while the interaction between dimers is much weaker. The shape of BoWSCP absorption spectrum in the Q_y band region (Fig. 3a) indicates the presence

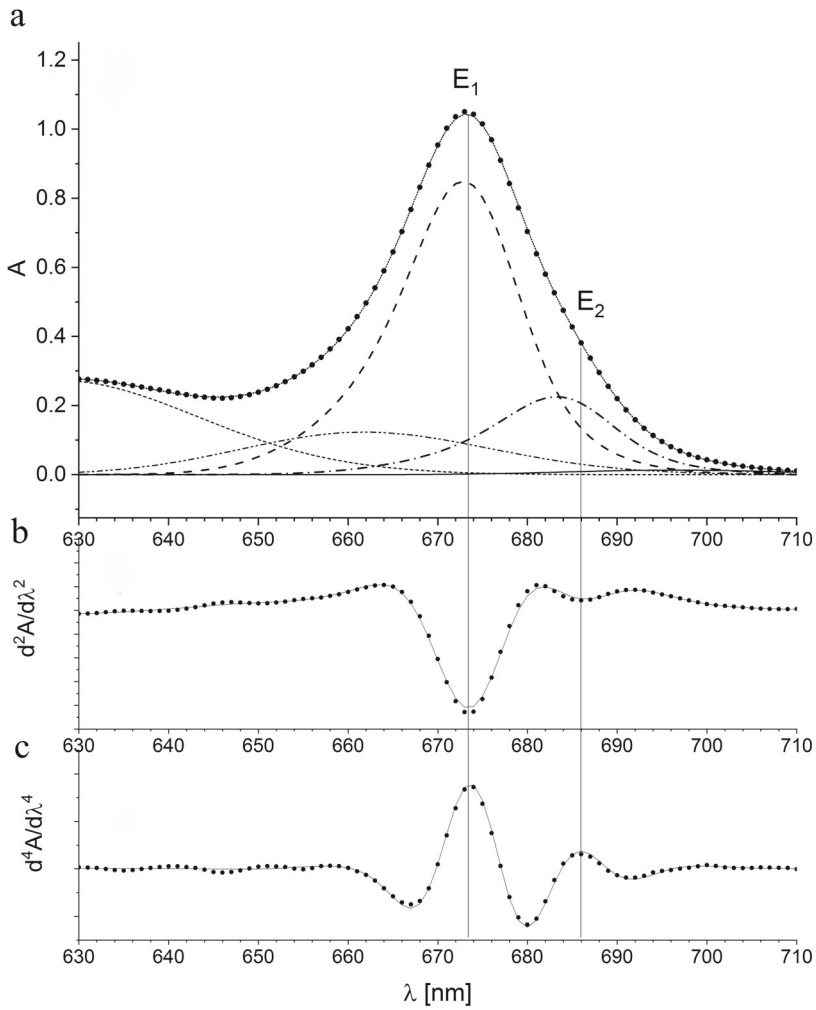

Fig. 3. The absorption spectrum (a), its second (b) and fourth (c) derivatives of BoWSCP holoform (dots). Solid lines represent a model spectrum, and dashed lines show its main Gaussian components. Vertical dashed lines show the maxima of the fourth derivative of the absorption spectrum.

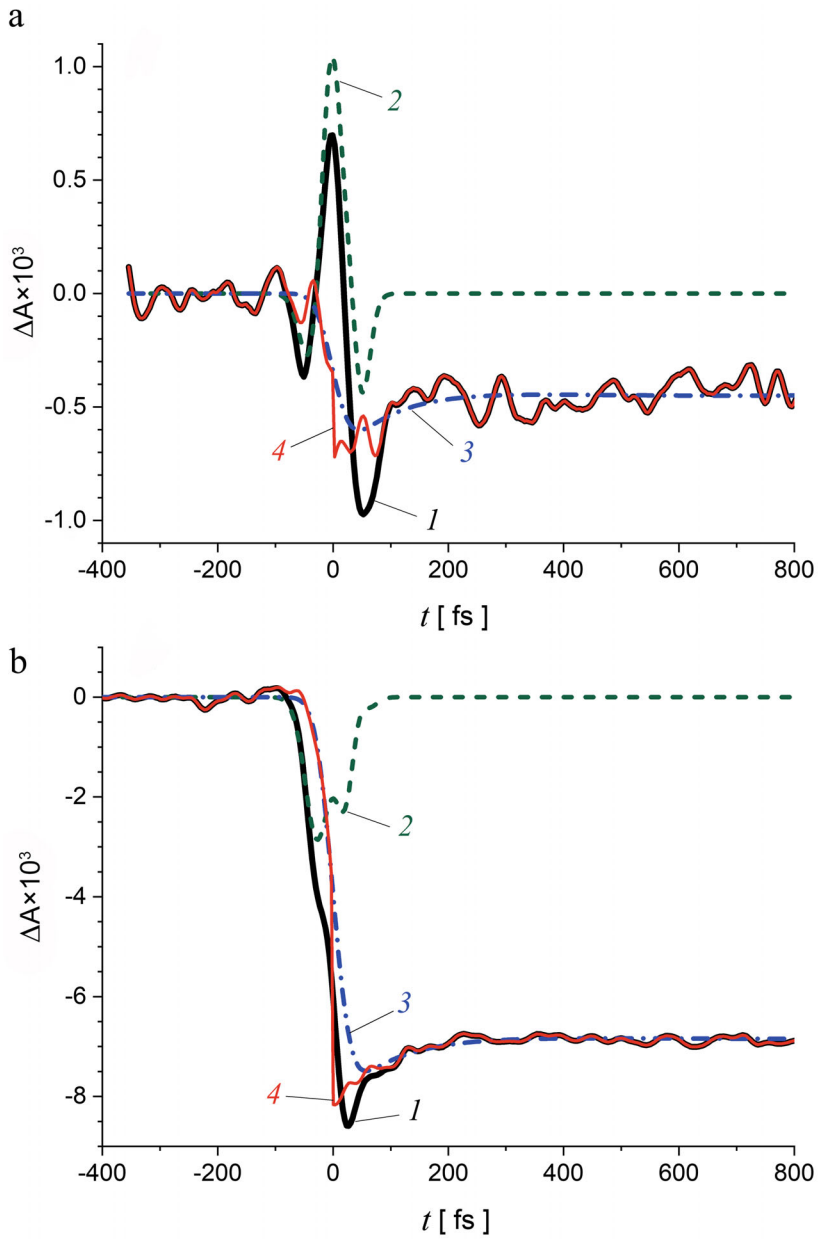

Fig. 4. Absorption changes of BoWSCP at the wavelengths of 450 nm (a) and 670 nm (b), induced by the pulse at 670 nm with a duration of 16 fs (the black solid line). The coherent artifact was approximated by superposition of the Gaussian function $G(t)$ (Eq. 1) and its derivatives G' and G'' (the dashed line), while the BoWSCP absorption changes were modelled by a combination of functions $\chi(t)$ and $\varepsilon(t,\tau_k)$ (the dot-dash line), with the parameter value $d = 24$ fs. The BoWSCP absorption response was obtained by subtraction of the coherent artifact (the red solid line).

of two exciton bands with peaks at 672 and 684 nm, corresponding to the minima of the second derivative (Fig. 3b) and maxima of the fourth derivative (Fig. 3c). Using the method proposed for analyzing WSCP spectra [20], the parameters of Chl *a* exciton interaction were determined by decomposing the BoWSCP absorption spectrum in the $Q_y(0,0)$ band region into Gaussian components. For an appropriate approximation of the $Q_y(0,0)$ band with intramolecular vibrational modes of the Chl tetrapyrrole macrocycle taken into account, additional Gaussian components were used in the high-energy region of the $Q_y(0,0)$ band [20, 36, 37]. The relative intensity of the main E_1 band peaking at 672 nm was 79%, while the contribution of the second E_2 band peaking at 684 nm was about 21%. Spectral characteristics of the E_3 state were not determined, and the E_4 state has zero intensity in the approximation of point dipoles.

Broadband femtosecond laser pump-probe spectroscopy was used for measuring the absorption dynamics of BoWSCP holoform, induced by excitation in the region of wavelengths of 430 and 670 nm. Excitation in these spectral regions is related mainly to Chl *a* (quantum yield is >98%) and only marginally to Chl *b* (<2%).

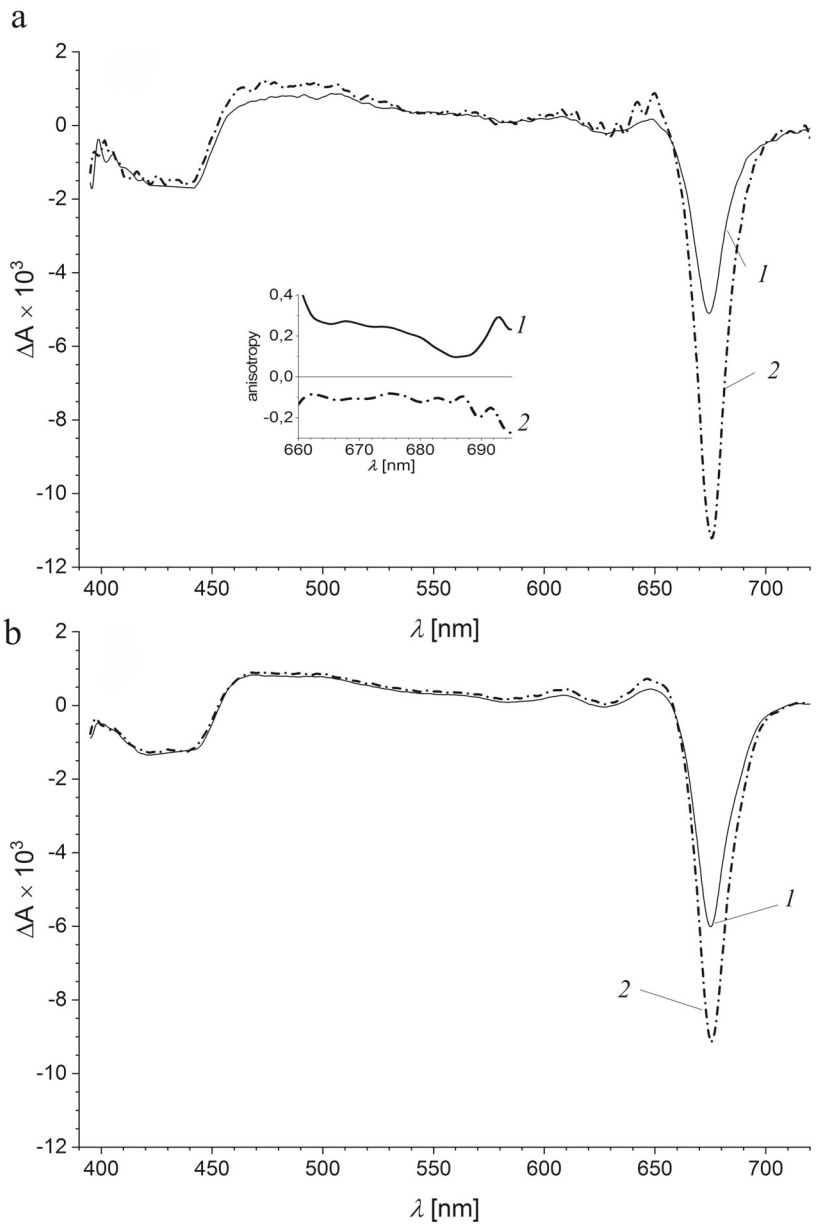

Fig. 5. Transient absorption spectra of BoWSCP at time delays of 50 fs (a) and 200 ps (b) induced by excitation at 430 nm (*1*) and 670 nm (*2*). The spectra are scaled in the Soret band region of 400-500 nm at the delay of 200 ps. The polarization angle is 54.7°. The inset shows the anisotropy coefficient in the Q_y band region

Figure 4 shows the coherent artifact (coherent spike) arising at short time delays due to nonlinear interactions of overlapping pump and probe pulses. The contribution of the coherent spike was divided from the absorption changes of the pigments according to the procedure described in "Materials and Methods". The BoWSCP absorption changes, starting from the time delay $t = 0$, were assessed by deconvolution of the resulting signal in accordance with equations (2) and (3).

Figure 5a shows transient absorption spectra of BoWSCP at a time delay of 50 fs, induced by the pulses at 430 nm (*1*, the solid line) and 670 nm (*2*, the dot-dash line). The 430 nm excitation is related mainly to the Chl transition $S_0 \rightarrow S_3$ into the third excited singlet state (the B_x band), while the 670 nm excitation produces the S_1 state (the Q_y band). This assignment is confirmed by a negative anisotropy observed in the region of the Q_y band upon excitation at 430 nm, where the anisotropy coefficient is close to the theoretical limit of –0.1 (see the inset in Fig. 5a).

The amplitude of the Q_y band bleaching in the BoWSCP transient absorption spectra in Fig. 5 is 3-5 times higher than that of the Soret band, while the amplitude of the Q_y band in the BoWSCP linear absorption spectrum in Fig. 1a is comparable to that of the Soret band. A transient absorption spectrum observed

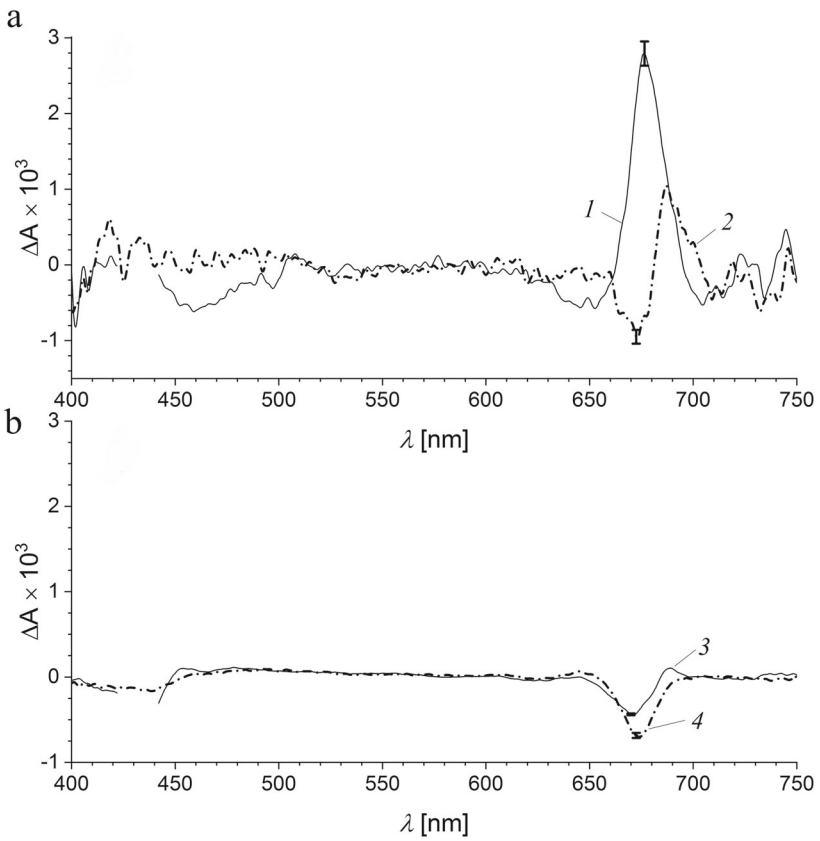

Fig. 6. Decay associated difference spectra of BoWSCP in the range of 100 fs (a) and 10 ps (b) after excitation at 430 nm (*1*, *3*) and 670 nm (*2*, *4*). Characteristic times: *1*) 83 fs, *2*) 105 fs, *3*) 19 ps, *4*) 14 ps. The marks on the graphs in the Q_y band area show the confidence intervals calculated using equation (8).

in the femtosecond measurements is the sum of three contributions. First is the spectrum of bleaching, which results from the disappearance of the ground state S_0, and its form corresponds to the inversed linear absorption spectrum. Second is the absorption spectrum of the emerging excited state S^*, and its contribution is always positive. Third is the spectrum of the reverse $S^* \rightarrow S_0$ transition, stimulated by emission, and for the lowest excited state its shape is close to the spontaneous fluorescence spectrum; its contribution is always negative. The main difference between the spectra (*1*) and (*2*) in Fig. 5a is visible in the Q_y band region, where the stimulated emission of the $S_1 \rightarrow S_0$ transition is observed, which does not exist during the lifetime of the S_3 state produced by the excitation at 430 nm. The less considerable difference between the spectra (*1*) and (*2*) in the region of 420-500 nm can be due to the stimulated emission of the $S_3 \rightarrow S_0$ transition.

Figure 5b shows transient absorption spectra at a time delay of 200 ps using the same notations: *1*) – excitation at 430 nm, *2*) – 670 nm. Within this time range the processes of $S_3 \rightarrow S_1$ intramolecular conversion and thermal equilibration between the four exciton states E_n of the tetrameric complex should be completed. The observed final spectra are close in the entire range, except for the Q_y band, where the bleaching amplitude after the excitation at 670 nm is much larger than that of the bleaching induced by the excitation at 430 nm.

The most significant BoWSCP absorption changes are related to the amplitude of the Q_y band bleaching after excitation at 430 nm. Its quantitative characteristics were determined by decomposing the absorption dynamics into exponential components (decay associated spectra, DAS, see "Materials and Methods"); decomposition revealed spectral transitions in the range of 100 fs and 10 ps (Fig. 6).

Figure 6a shows the difference decay spectra for the femtosecond range. After excitation at 430 nm the main spectral changes occur with the characteristic time of 83 ± 9 fs. They can be attributed to the nonradiative intramolecular $S_3 \rightarrow S_1$ conversion, as a result of which the stimulated emission disappears in the Soret band region (450-480 nm) but appears in the region of the Q_y band (670-690 nm). When BoWSCP is excited in the Q_y band region at 670 nm, clearly distinguishable small spectral changes occur with a characteristic time of 105 ± 10 fs, and they can be attributed to the relaxation transition between the two excitonic substates E_1 and E_2 of the Q_y band of Chl *a* dimer.

In the picosecond range, significant absorption changes occur with a characteristic time of ~16 ps. The DAS calculated for excitation at 430 nm (characteristic time 19 ± 3 ps) and 670 nm (characteristic time 14 ± 2 ps) are close throughout the entire spectral range (Fig. 6b) and are associated with insignificant absorption recovering in the region of the Q_y band with a maximum around 675 nm. Possible interpretations of these changes will be considered further.

To provide quantitative characteristics of photochemical processes observed by means of femtosecond measurements in the system of excitonically coupled pigments, transient absorption (TA) was decomposed into three components: ground state bleaching (GSB), excited state absorption (ESA), and stimulated emission (SE). The probability of light absorption with the quantum energy $\hbar\omega_0$ by a separate pigment molecule is proportional to square of the dipole moment $|\mu|^2$ for its transition from the ground state to the excited state (dipole strength of the transition). For Chl *a* monomer in protein, the dipole moment of $S_0 \rightarrow S_1$ transition is equal to 5.5 D [38]. The pump pulse causes transition of ΔN molecules in the sample from the ground state to the excited state. The probe pulse is split into two beams: one beam passes through a non-excited sample, and another beam passes through the excitation region. The difference in beams intensity determines the difference absorption. In the excitation region the number of molecules in the ground state is decreased by ΔN. Therefore, absorption at the frequency ω_0 in this region is proportional to the transition dipole strength, $\Delta A_{GSB} \propto |\mu|^2$. At the same time, there is light emission of the reverse $S_1 \rightarrow S_0$ transition stimulated by the light wave, its probability is also proportional to the dipole moment strength, so the absorption at the frequency ω_0 is additionally decreased by the same value, $\Delta A_{SE} \propto |\mu|^2$. For an ideal two-level system, the ratio $\beta = \Delta A_{SE}/\Delta A_{GSB}$ is equal to one [39]; for Chl *a* in various solvents the estimate was $\beta \approx 0.9$ [40, 41].

For excitonically coupled pigments the situation is way more complex. The dipole moment of excitonically coupled pigments represents a linear sum of the dipole moments of monomers [42]. In the BoWSCP crystallographic structure [18], the dipole moments of monomers $\boldsymbol{\mu}_k$ are almost parallel to the crystallographic axis X, while projections of the moments to axes Y and Z are much smaller in terms of absolute values [13]. In the first approximation they may be assumed to be equal to zero. Projections of the monomer dipole moment to crystallographic axes are shown schematically in Fig. 2.

Quantitative description of light interaction with Chl molecules in the BoWSCP tetramer raises a question of basic nature: is the emerging excited state localized within the dimer (the coupling energy of ~100 cm^{-1}), or is it delocalized across the entire tetrameric complex (the coupling energy of ~10 cm^{-1})? The femtosecond measurements enable determining the degree of excited state delocalization, i.e., the number of Chl molecules effectively involved in the exciton coupling.

For a symmetric dimer, the dipole moments of the transitions to two possible excited states E_+ and E_- are equal [43] (10):

$$\mathbf{M}_{\pm} = \frac{1}{\sqrt{2}} (\boldsymbol{\mu}_1 \pm \boldsymbol{\mu}_2). \quad (10)$$

It should be noted that the excitonic interaction of monomers does not change the total dipole strength of the complex: $|\mathbf{M}_+|^2 + |\mathbf{M}_-|^2 = \mu_1^2 + \mu_2^2$, therefore, the integral amplitude of the linear absorption spectrum remains constant. Due to the geometry of the BoWSCP tetramer, the dipole strength of the transition to the E_+ state is equal to $|\mathbf{M}_+|^2 \cong \mu_1^2 + \mu_2^2 = 2\mu_1^2$, while the dipole strength of the transition to the E_- state is close to zero; therefore, when BoWSCP is excited by a broadband pulse centered at a wavelength of 670 nm (half-width of 50 nm, time duration of 16 fs), in the initial distribution of arising exciton states, the E_+ state significantly predominates.

In this case, the total amplitude of bleaching ΔA_{BL} in the initial transition spectrum near the exciton splitting band at frequency ω_0 is (11):

$$\Delta A_{BL} = \Delta A_{GSB} + \Delta A_{SE} \propto (1 + \beta)2\mu_1^2 \approx 4\mu_1^2. \quad (11)$$

In the rest of the spectral range, the bleaching of the ground state is proportional to the dipole strength of the free monomer (12):

$$\Delta A_{GSB}(\omega) \propto \mu_1^2. \quad (12)$$

For a symmetric tetramer, the transition dipole moments of four possible exciton states are found by a unitary transformation [42], the moment with the largest amplitude is equal to (13):

$$\mathbf{M}_1 = ½(\boldsymbol{\mu}_1 + \boldsymbol{\mu}_2 - \boldsymbol{\mu}_3 - \boldsymbol{\mu}_4). \quad (13)$$

In this case, the total bleaching amplitude of the transition spectrum near the exciton splitting band is (14):

$$\Delta A_{BL} \propto 8\mu_1^2. \quad (14)$$

In general, the number of excitonically coupled molecules, n_{excited}, between which the excited state is delocalized, can be determined by the ratio of the total bleaching amplitude of the transition spectrum at the frequency of the exciton transition ω_0 and the amplitude of the linear spectrum, which does not take into account the selective nature of the complex excitation (15):

$$n_{\text{excited}} = ½\Delta A_{BL}/\Delta A_{GSB}. \quad (15)$$

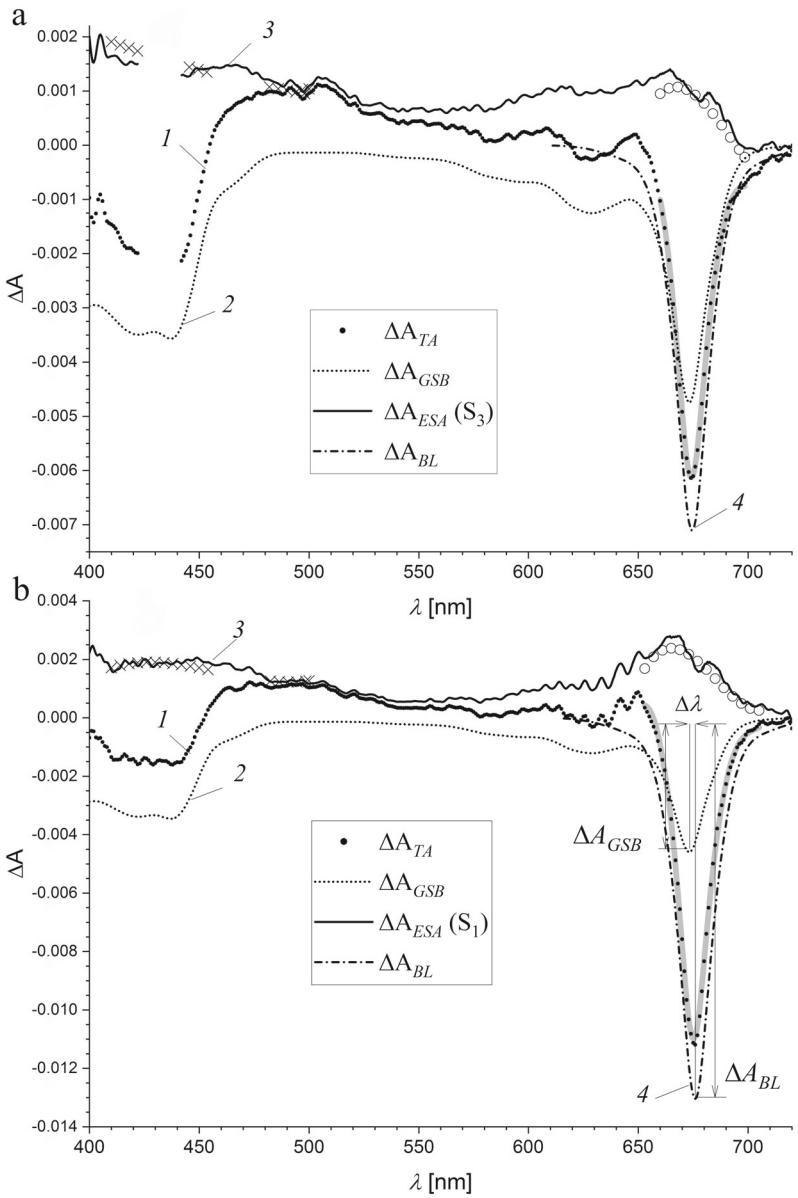

Fig. 7. Decomposition of the BoWSCP transient absorption spectrum (*1* – Transient Absorption, *TA*) into components of ground state bleaching (*2* – Ground State Bleaching, *GSB*), excited state absorption (*3* – Excited State Absorption, ESA) and bleaching in the stimulated emission region (*4* – Bleach, *BL*). Transient absorption spectra were obtained at a delay of 50 fs after excitation at 430 nm (a) and 670 nm (b). The bleaching spectrum (*2*) was normalized based on the *TA* spectrum (*1*) in the region of 400-500 nm, taking into account approximation of the excited state spectrum by a cubic polynomial function (×). The model bleaching spectrum in the region of 650-700 nm near the stimulated emission (*4*) in the range $\Delta A_{BL} = \Delta A_{GSB} + \Delta A_{SE}$ was represented by a sum $\Delta A_{BL} = n_{\text{excited}} \cdot (\Delta A_{GSB} + \Delta A_{SE})$ of the linear absorption spectrum and its mirror reflection relative to the maximum of the absorption band Q_y peak and the Stokes shift $\Delta\lambda$. The model spectrum amplitude n_{excited} was determined by linear regression using polynomial approximation of the excited state spectrum (○). The thick gray line shows the result of such decomposition.

When BoWSCP is excited at 670 nm, the amplitude of the ground state bleaching ΔA_{GSB} can be determined from the Soret band. In Fig. 7 dots show the transition spectra of BoWSCP at a time delay of 50 fs after excitation at wavelengths of 430 nm (a) and 670 nm (b).

In the region of 400-500 nm, the transition spectra (*1*) are close in shape to the absorption spectrum of BoWSCP (*2*), with the exception of the region of 450-480 nm, where absorption of Chl *b* and stimulated emission of Chl *a* from the S_3 state predominate. Assuming that the absorption spectra of the excited states S_1 and S_3 are smooth functions in the specified wavelength range and can be correctly described by third-degree polynomials $P_3(\lambda)$, the transition spectra were approximated by the expression (16):

$$\Delta A_{TA}(\lambda) = \xi \cdot \Delta A_{GSB}(\lambda) + P_3(\lambda), \qquad (16)$$

in which the scaling factor ξ and the coefficients of the cubic polynomial P_3 were found by the standard

solution to the linear regression problem. The absorption spectra of excited states in the region where the stimulated emission is absent are found as the difference $\Delta A_{ESA}(\lambda) = \Delta A_{TA}(\lambda) - \xi \cdot \Delta A_{GSB}(\lambda)$. Figure 7 shows the obtained bleaching spectra of the ground state (*2*), the polynomial functions P_3 (×), and the absorption spectra of excited states (*3*).

The model bleaching spectrum near the Qy band (*4*) was represented by the sum of the linear absorption spectrum taken with the opposite sign $\Delta A_{GSB}(\lambda)$, and its mirror reflection relative to the maximum of the Qy band $\Delta A_{SE}(\lambda)$. Since the position of the 0-0 transition remained unknown, the value of the Stokes shift $\Delta\lambda$ of the *SE* spectrum was found by nonlinear minimization of the total model spectrum (17):

$$\Delta A_{TA}(\lambda) = n_{\text{excited}} \cdot \xi \cdot [\Delta A_{GSB}(\lambda) + \\ + \Delta A_{GSB}(\lambda_0 + \Delta\lambda - \lambda)] + P_3(\lambda). \quad (17)$$

The effective number of excitonically coupled molecules n_{excited} and the coefficients of the polynomial function P_3 were found by linear regression. Gray thick line in Fig. 7 presents the result of this decomposition. When excited at 430 nm, the observed Q_y band bleaching amplitude ΔA_{BL} is only slightly larger than the ground state bleaching amplitude ΔA_{GSB}, while when excited at 670 nm, the ΔA_{BL} amplitude is three times the amplitude ΔA_{GSB}.

Figure 8a shows time dependence of the bleaching amplitude of the Soret band (*1*, *2*) and the Q_y band (*3*, *4*), induced by BoWSCP excitation at 430 nm (solid lines) and 670 nm (dot-dash lines). Absorption changes in the time range of 100 fs with excitation at 430 nm (*3*) reflects stimulated emission which appears as a result of electronic transition $S_3 \rightarrow S_1$, with a characteristic time of 80 fs. As it was noted above, the bleaching amplitude of the Q_y band after excitation in the region of 430 nm remains much lower throughout the time interval than the amplitude of this band after excitation at 670 nm. The high bleaching amplitude of Q_y band after excitation at 670 nm throughout the time interval is another feature: its amplitude is three times higher than that of the Soret band.

Figure 8b shows changes in the effective number n_{excited} of exciton-coupled Chl molecules in the course of time, which is calculated according to the equation (15) for two BoWSCP excitation variants. Between these molecules, the excited state of the tetramer is delocalized. For short delays in the case of excitation at 670 nm, n_{excited} is close to 2, i.e., BoWSCP acts as an exciton-coupled dimer. In case of excitation at 430 nm at short delays, n_{excited} is close to 0.5. As it was noted above, this means that the excited state S_3 prevails in these conditions.

Finally, Fig. 8c shows changes in the anisotropy coefficient, $r = (\Delta A_{\parallel} - \Delta A_{\perp}) / (\Delta A_{\parallel} + 2\Delta A_{\perp})$, calculated in the Q_y band region for two excitation variants. The changes in the Q_y band bleaching amplitude at the timescale of ~100 fs are almost unrelated to the anisotropy changes.

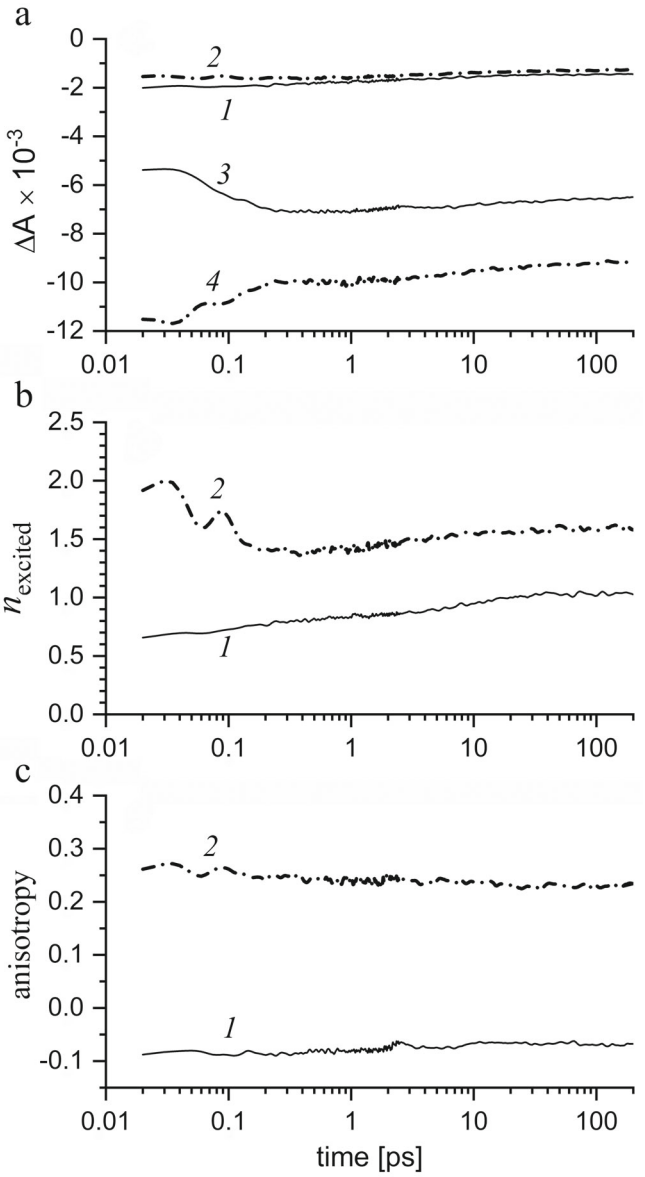

Fig. 8. Changes in the main parameters characterizing the excited state of BoWSCP tetrameric complex in the course of time. a) Bleaching amplitude of the Soret band (*1*, *2*) and the Q_y band (*3*, *4*) after excitation at 430 nm (*1*, *3*) and 670 nm (*2*, *4*). b) The effective number of excitonically coupled Chl molecules calculated by to the equation (15) for excitation at 430 nm (*1*) and 670 nm (*2*). c) The anisotropy coefficient calculated in the Q_y band region for excitation at 430 nm (*1*) and 670 nm (*2*).

DISCUSSION

WSCP proteins represent a uniquely organized model system of exciton-coupled chlorophyll molecules [11], which allows research into the mechanisms

of excitation energy transfer between pigments [12-14] and the interaction of excited pigments with surrounding proteins [15-17]. Energy exchange between the electron subsystem and nuclei vibration triggers the evolution of electronic states [44, 45]. The efficiency of energy exchange between exciton states and phonon modes depends on spectral density of nuclei vibrational states. To determine this experimentally, spectral hole burning [46-48] and time-resolved fluorescence spectroscopy [10] were used. Chl *a* vibron bands comprise over 40 modes within the range of 1500 to 260 cm^{-1} [49-51]. The dipole–dipole interaction of adjacent Chl *a* molecules in the BoWSCP tetramer obtained by joint decomposition of absorption and circular dichroism spectra is ~100 cm^{-1} [20], which allows considering the delocalized excited states of pigments in terms of the exciton theory [42]. The value of exciton interaction of dimers of WSCP tetramer calculated using the X-ray structure of the complex is ~10vcm^{-1} [13], which allows describing energy transfer between dimers using Förster theory [52].

Measurement of absorption dynamics of WSCP proteins of subclasses IIa (BoWSCP, from *Brassica oleracea*) and IIb (LvWSCP, from *Lepidium virginicum*) in the femtosecond range had been carried out in the Q_y band region using pump-probe spectroscopy [14] and 2D spectroscopy [12, 13]. Theiss et al. measured absorption changes in the BoWSCP complex contained 20-30% Chl *b*, and in that system, transfer of excitation from Chl *b* to Chl *a* with a characteristic time of 400 fs was registered [14]. That process was considered as an exciton relaxation of heterodimer Chl *a*-Chl *b*, but later the exciton relaxation of the heterodimer was shown to occur faster than in 100 fs, and processes with the time of 250-400 fs were ascribed to the energy transfer between dimers [12]. The methods of 2D spectroscopy were used for studying absorption dynamics of LvWSCP and BoWSCP homotetramers containing 100% Chl *a* [13]. In both systems monoexponential absorption dynamics with characteristic times of 70 and 100 fs, respectively, were observed in the subpicosecond scale; these processes were interpreted as the $E_1 \rightarrow E_2$ relaxation to the lowest exciton state [13]. Calculations with the modified Redfield theory predict that equilibrium between exciton states should be achieved within this time range [15]. The spectral transition with the time of 110 fs, observed in case of BoWSCP excitation at 670 nm (Fig. 6a, spectrum *2*) matches the previously obtained data.

In this work the absorption dynamics of Chl *a* tetrameric complex was first measured in the wide spectral range of 400-750 nm with a time resolution of 20 fs. This made is possible to register the intramolecular conversion of Chl *a* from the excited state S_3 to S_1, to analyze relaxation dynamics of exciton-coupled molecules of Chl *a*, and to provide quantitative characteristics of distribution between the E_1 and E_2 excitonic states related to the Q_y band of Chl *a* dimer. All that was possible within a single experimental system.

Quantitative comparison of absorption dynamics in the Soret and Q_y band regions is required for properly interpreting the data obtained with large photosynthetic complexes. For instance, the bleaching amplitude of Chl *a* in the Q_y band region in primary transient absorption spectra of photosystem I from cyanobacterium *Thermosynechococcus elongatus* in case of excitation in the far-red region [53], and of Chl *a* and Chl *f* in similar spectra of photosystem I from cyanobacterium *Fischerella thermalis* PCC 7521 [54] is 3-6 times higher than the bleaching amplitude of Soret bands. Meanwhile, in similar spectra of photosystem I from cyanobacterium *Synechocystis* sp. PCC 6803 the bleaching amplitude of the Q_y band is only slightly higher than that of the Soret band [55]. Van Stokkum et al. assumed that the high amplitude of the Q_y band in the primary spectra of photosystem I is an evidence for quenching of most excited states by preoxidized chlorophyll of the special pair P700 [56]. However, the light-harvesting complexes of photosystem I of cyanobacteria *T. elongatus* and *F. thermalis* PCC 7521 contain exciton-coupled dimers and trimers of Chl with maximum absorption in the far-red region, as distinct from *Synechocystis* sp. PCC 6803 [57-60]. The results obtained in this paper regarding the impact of exciton coupling on the bleaching amplitude of the Q_y band (Fig. 8) explain the observed effects by structural features of the light-harvesting complexes.

Presented in Fig. 8, the dependencies of the bleaching amplitude of the Soret band and the Q_y band together with the determined $n_{excited}$ coefficient representing the number of exciton-coupled Chl molecules provide several conclusions about the physical and chemical properties of BoWSCP excited states.

1. In case of BoWSCP excitation in the Q_y band region, the highest excitonic state E_1 with the peak at 672 nm is predominantly formed. The thermal equilibrium between the E_1 and E_2 states (peak at about 684 nm) is established at the characteristic time $\tau_1 = 105 \pm 10$ fs. However, the contribution of the high-energy E_1 state prevails over the low-energy E_2 state in the entire time interval of hundreds of picoseconds (the relative contribution is $\geqslant$80%). The population inversion can be due to a considerable contribution of entropy to the difference in free energy of the E_1 and E_2 states. This implicates a strong electronic interaction between BoWSCP monomers, which takes place in case of considerable overlapping of wave functions of excited states. In such strongly coupled dimers, resonant charge-transfer states arise, which determine a strong electron-phonon coupling [61, 62].

2. When BoWSCP is excited in the Soret band region, the electronic state S_3 (also designated as B_x) is predominantly produced, which is transformed to the S_1 state by a process of intramolecular conversion

with the characteristic time of 83 ± 9 fs. However, the stimulated emission in the later state is characterized by the amplitude which is almost halved compared to the equilibrium S_1 state formed after excitation at 670 nm. The decreased stimulated emission amplitude can result from an ultrafast photochemical reaction of Chl oxidation and reduction of a tryptophan residue, "competing" with the intramolecular conversion reaction. In this case a reverse recombination reaction of Chl^+Trp^- ion-radical pair can take more than 200 ps. The photoreduction of tryptophan $Chl^*\rightarrow Chl^+Trp^-$ was registered for LvWSCP by spectral hole burning at the temperature of 4 K in an hour timescale and with a low quantum yield [47]. It can thus be assumed that spectral changes with the characteristic time $\tau_2 = 16 \pm 3$ ps (Fig. 6b) can result from acceleration of this photochemical reaction at the temperature of 279 K.

3. An increased bleaching amplitude of the Q_y band in relation to the Soret band was observed in transient absorption spectra of photosystem I of various cyanobacteria with specific excitation of long-wavelength chlorophyll forms [53, 54, 63]. Long-wavelength chlorophyll forms in the light-harvesting antenna and the reaction center of photosystem I arise due to formation of excitonically coupled Chl dimers and trimers [60, 64, 65], which obviously has the molecule structure similar to the architecture of chlorophyll molecules in the WSCP complex.

Contributions. D.A.Ch. analysis of spectral measurement results; K.V.N., Yu.N.O., and Yu.V.M. production, recovery, and biochemical characterization of BoWSCP preparations; F.E.G., I.V.Sh., and A.V.A. development of a mathematical apparatus, methods and performing femtosecond measurements; M.S.K. and V.A.N. concept development. All authors made a considerable contribution to the manuscript.

Funding. This research was funded by the Russian Science Foundation (grant no. 21-74-20155).

Acknowledgments. The authors thank A. L. Dobryakov for assistance in developing the coherent artifact approximation method and setting the femtosecond device. In this paper the equipment (the femtosecond device) provided by the Center for Collective Use of N. N. Semenov Federal Research Center for Chemical Physics, Russian Academy of Sciences "Analysis of Chemical and Biological Systems and Natural Materials: Mass Spectral Microscopy and Femtosecond Laser Microscopy and Spectroscopy" (registration number: 506694). The expression vector pET-24b with the embedded BoWSCP gene was kindly provided by Prof. Dr. Harald Paulsen (Institute of Molecular Physiology, Johannes Gutenberg University Mainz, Germany)

Ethics declarations. The authors declare no conflict of interests in financial or any other sphere. This article does not contain any studies with human participants or animals performed by any of the authors.

REFERENCES

1. Charlton, A., and Zachariou, M. (2007) Immobilized metal ion affinity chromatography of histidine-tagged fusion proteins, *Methods Mol. Biol.*, **421**, 137-149, doi: 10.1007/978-1-59745-582-4_10.
2. Cherepanov, D. A., Semenov, A. Y., Mamedov, M. D., Aybush, A. V., Gostev, F. E., Shelaev, I. V., Shuvalov, V. A., and Nadtochenko, V. A. (2022) Current state of the primary charge separation mechanism in photosystem I of cyanobacteria, *Biophys. Rev.*, **14**, 805-820, doi: 10.1007/s12551-022-00983-1.
3. Murata, T., Toda, F., Uchino, K., and Yakushiji, E. (1971) Water-soluble chlorophyll protein of *Brassica oleracea* var. botrys (cauliflower), *Biochim. Biophys. Acta Bioenerg.*, **245**, 208-215, doi: 10.1016/0005-2728(71)90023-5.
4. Satoh, H., Nakayama, K., and Okada, M. (1998) Molecular cloning and functional expression of a water-soluble chlorophyll protein, a putative carrier of chlorophyll molecules in cauliflower, *J. Biol. Chem.*, **273**, 30568-30575, doi: 10.1074/jbc.273.46.30568.
5. Takahashi, S., Yanai, H., Nakamaru, Y., Uchida, A., Nakayama, K., and Satoh, H. (2012) Molecular cloning, characterization and analysis of the intracellular localization of a water-soluble chl-binding protein from brussels sprouts (*Brassica oleracea* var. gemmifera), *Plant Cell Physiol.*, **53**, 879-891, doi: 10.1093/pcp/pcs031.
6. Takahashi, S., Yanai, H., Oka-Takayama, Y., Zanma-Sohtome, A., Fujiyama, K., Uchida, A., Nakayama, K., and Satoh, H. (2013) Molecular cloning, characterization and analysis of the intracellular localization of a water-soluble chlorophyll-binding protein (WSCP) from Virginia pepperweed (*Lepidium virginicum*), a unique WSCP that preferentially binds chlorophyll *b in vitro*, *Planta*, **238**, 1065-1080, doi: 10.1007/s00425-013-1952-7.
7. Satoh, H., Uchida, A., Nakayama, K., and Okada, M. (2001) Water-soluble chlorophyll protein in Brassicaceae plants is a stress-induced chlorophyll-binding protein, *Plant Cell Physiol.*, **42**, 906-911, doi: 10.1093/pcp/pce117.
8. Horigome, D., Satoh, H., Itoh, N., Mitsunaga, K., Oonishi, I., Nakagawa, A., and Uchida, A. (2007) Structural mechanism and photoprotective function of water-soluble chlorophyll-binding protein, *J. Biol. Chem.*, **282**, 6525-6531, doi: 10.1074/jbc.M609458200.
9. Maleeva, Y. V., Neverov, K. V., Obukhov, Y. N., and Kritsky, M. S. (2019) Water soluble chlorophyll-binding proteins of plants: structure, properties and functions, *Mol. Biol. (Mosk)*, **53**, 998-1011, doi: 10.1134/S0026898419060120.
10. Schmitt, F. J., Trostmann, I., Theíss, C., Pieper, J., Renger, T., Fuesers, J., Hubrich, E. H., Paulsen, H., Eichler, H. J., and Renger, G. (2008) Excited state dynamics in recombinant water-soluble chlorophyll proteins (WSCP) from cauliflower investigated by transient fluorescence spectroscopy, *J. Phys. Chem. B*, **112**, 13951-13961, doi: 10.1021/jp8024057.

11. Renger, G., Pieper, J., Theiss, C., Trostmann, I., Paulsen, H., Renger, T., Eichler, H. J., and Schmitt, F. J. (2011) Water soluble chlorophyll binding protein of higher plants: A most suitable model system for basic analyses of pigment–pigment and pigment–protein interactions in chlorophyll protein complexes, *J. Plant Physiol.*, **168**, 1462-1472, doi: 10.1016/j.jplph.2010.12.005.
12. Alster, J., Lokstein, H., Dostál, J., Uchida, A., and Zigmantas, D. (2014) 2D spectroscopy study of water-soluble chlorophyll-binding protein from lepidium virginicum, *J. Phys. Chem. B*, **118**, 3524-3531, doi: 10.1021/jp411174t.
13. Fresch, E., Meneghin, E., Agostini, A., Paulsen, H., Carbonera, D., and Collini, E. (2020) How the protein environment can tune the energy, the coupling, and the ultrafast dynamics of interacting chlorophylls: the example of the water-soluble chlorophyll protein, *J. Phys. Chem. Lett.*, **11**, 1059-1067, doi: 10.1021/acs.jpclett.9b03628.
14. Theiss, C., Trostmann, I., Andree, S., Schmitt, F. J., Renger, T., Eichler, H. J., Paulsen, H., and Renger, G. (2007) Pigment–pigment and pigment–protein interactions in recombinant water-soluble chlorophyll proteins (WSCP) from cauliflower, *J. Phys. Chem. B*, **111**, 13325-13335, doi: 10.1021/jp0723968.
15. Renger, T., Trostmann, I., Theiss, C., Madjet, M. E., Richter, M., Paulsen, H., Eichler, H. J., Knorr, A., and Renger, G. (2007) Refinement of a structural model of a pigment–protein complex by accurate optical line shape theory and experiments, *J. Phys. Chem. B*, **111**, 10487-10501, doi: 10.1021/jp0717241.
16. Friedl, C., Fedorov, D. G., and Renger, T. (2022) Towards a quantitative description of excitonic couplings in photosynthetic pigment-protein complexes: Quantum chemistry driven multiscale approaches, *Phys. Chem. Chem. Phys.*, **24**, 5014-5038, doi: 10.1039/d1cp03566e.
17. Lahav, Y., Noy, D., and Schapiro, I. (2021) Spectral tuning of chlorophylls in proteins – electrostatics vs. ring deformation, *Phys. Chem. Chem. Phys.*, **23**, 6544-6551, doi: 10.1039/d0cp06582j.
18. Agostini, A., Meneghin, E., Gewehr, L., Pedron, D., Palm, D. M., Carbonera, D., Paulsen, H., Jaenicke, E., and Collini, E. (2019) How water-mediated hydrogen bonds affect chlorophyll *a*/*b* selectivity in water-soluble chlorophyll protein, *Sci. Rep.*, **9**, 18255, doi: 10.1038/s41598-019-54520-4.
19. Bednarczyk, D., Dym, O., Prabahar, V., Peleg, Y., Pike, D. H., and Noy, D. (2016) Fine tuning of chlorophyll spectra by protein-induced ring deformation, *Angew. Chemie Int. Ed.*, **55**, 6901-6905, doi: 10.1002/anie.201512001.
20. Hughes, J. L., Razeghifard, R., Logue, M., Oakley, A., Wydrzynski, T., and Krausz, E. (2006) Magneto-optic spectroscopy of a protein tetramer binding two exciton-coupled chlorophylls, *J. Am. Chem. Soc.*, **128**, 3649-3658, doi: 10.1021/ja056576b.
21. Obukhov, Y. N., Neverov, K. V., Maleeva, Y. V., and Kritsky, M. S. (2023) Chlorophyll a dimers bound in the water-soluble protein BoWSCP photosensitize the reduction of cytochrome *c*, *Dokl. Biochem. Biophys.*, **509**, 60-64, doi: 10.1134/S1607672923700126.
22. Takahashi, S., Uchida, A., Nakayama, K., and Satoh, H. (2014) Three-step photoconversion of only three subunits of the water-soluble chlorophyll-binding protein tetramer from *Chenopodium album*, *Protein J.*, **33**, 337-343, doi: 10.1007/s10930-014-9565-y.
23. Kelly, S. M., Jess, T. J., and Price, N. C. (2005) How to study proteins by circular dichroism, *Biochim. Biophys. Acta Proteins Proteomics*, **1751**, 119-139, doi: 10.1016/j.bbapap.2005.06.005.
24. Bradford, M. M. (1976) A rapid and sensitive method for the quantitation of microgram quantities of protein utilizing the principle of protein-dye binding, *Anal. Biochem.*, **72**, 248-254, doi: 10.1016/0003-2697(76)90527-3.
25. Cherepanov, D. A., Shelaev, I. V., Gostev, F. E., Mamedov, M. D., Petrova, A. A., Aybush, A. V., Shuvalov, V. A., Semenov, A. Y., and Nadtochenko, V. A. (2017) Mechanism of adiabatic primary electron transfer in photosystem I: Femtosecond spectroscopy upon excitation of reaction center in the far-red edge of the Q Y band, *Biochim. Biophys. Acta Bioenerg.*, **1858**, 895-905, doi: 10.1016/j.bbabio.2017.08.008.
26. Dobryakov, A. L., Pérez Lustres, J. L., Kovalenko, S. A., and Ernsting, N. P. (2008) Femtosecond transient absorption with chirped pump and supercontinuum probe: Perturbative calculation of transient spectra with general lineshape functions, and simplifications, *Chem. Phys.*, **347**, 127-138, doi: 10.1016/j.chemphys.2007.11.003.
27. Golubeva, E. N., Zubanova, E. M., Melnikov, M. Y., Gostev, F. E., Shelaev, I. V., and Nadtochenko, V. A. (2014) Femtosecond spectroscopy and TD-DFT calculations of $CuCl_4^{2-}$ excited states, *Dalt. Trans.*, **43**, 17820-17827, doi: 10.1039/C4DT01409J.
28. Dobryakov, A. L., Kovalenko, S. A., Weigel, A., Prez-Lustres, J. L., Lange, J., Müller, A., and Ernsting, N. P. (2010) Femtosecond pump/supercontinuum-probe spectroscopy: Optimized setup and signal analysis for single-shot spectral referencing, *Rev. Sci. Instrum.*, **81**, 113106, doi: 10.1063/1.3492897.
29. Kovalenko, S. A., Dobryakov, A. L., Ruthmann, J., and Ernsting, N. P. (1999) Femtosecond spectroscopy of condensed phases with chirped supercontinuum probing, *Phys. Rev. A At. Mol. Opt. Phys.*, **59**, 2369-2384, doi: 10.1103/PhysRevA.59.2369.
30. Šimůnek, J. and Hopmans, J.W. (2002). 1.7 Parameter Optimization and Nonlinear Fitting, in *Methods of Soil Analysis* (eds Dane, J. H. and Clarke Topp, G.), pp. 139-157, doi: 10.2136/sssabookser5.4.c7.
31. Clementson, L. A., and Wojtasiewicz, B. (2019) Dataset on the absorption characteristics of extracted phytoplankton pigments, *Data Br.*, **24**, 103875, doi: 10.1016/j.dib.2019.103875.
32. Sirohiwal, A., Berraud-Pache, R., Neese, F., Izsák, R., and Pantazis, D. A. (2020) Accurate computation of the absorption spectrum of chlorophyll *a* with pair natural

orbital coupled cluster methods, *J. Phys. Chem. B*, **124**, 8761-8771, doi: 10.1021/acs.jpcb.0c05761.
33. Gouterman, M. (1961) Spectra of porphyrins, *J. Mol. Spectrosc.*, **6**, 138-163, doi: 10.1016/0022-2852(61)90236-3.
34. Bricker, W. P., Shenai, P. M., Ghosh, A., Liu, Z., Enriquez, M. G. M., Lambrev, P. H., Tan, H. S., Lo, C. S., Tretiak, S., Fernandez-Alberti, S., and Zhao, Y. (2015) Non-radiative relaxation of photoexcited chlorophylls: theoretical and experimental study, *Sci. Rep.*, **5**, 13625, doi: 10.1038/srep13625.
35. Götze, J. P., Anders, F., Petry, S., Witte, J. F., and Lokstein, H. (2022) Spectral characterization of the main pigments in the plant photosynthetic apparatus by theory and experiment, *Chem. Phys.*, **559**, 111517, doi: 10.1016/j.chemphys.2022.111517.
36. Umetsu, M., Wang, Z. Y., Kobayashi, M., and Nozawa, T. (1999) Interaction of photosynthetic pigments with various organic solvents. Magnetic circular dichroism approach and application to chlorosomes, *Biochim. Biophys. Acta Bioenerg.*, **1410**, 19-31, doi: 10.1016/S0005-2728(98)00170-4.
37. Shipman, L. L., Cotton, T. M., Norris, J. R., and Katz, J. J. (1976) An analysis of the visible absorption spectrum of chlorophyll *a* monomer, dimer,and oligomers in solution, *J. Am. Chem. Soc.*, **98**, 8222-8230, doi: 10.1021/ja00441a056.
38. Cherepanov, D. A., Milanovsky, G. E., Aybush, A. V., and Nadtochenko, V. A. (2023) Dipole moment of the S0-S1 chlorophyll a transition in solvents with varied refraction index, *Russ. J. Phys. Chem. B*, **17**, 584-593, doi: 10.1134/S1990793123030181.
39. Berera, R., van Grondelle, R., and Kennis, J. T. M. (2009) Ultrafast transient absorption spectroscopy: principles and application to photosynthetic systems, *Photosynth. Res.*, **101**, 105-118, doi: 10.1007/s11120-009-9454-y.
40. Cherepanov, D. A., Gostev, F. E., Shelaev, I. V., Aibush, A. V., Mamedov, M. D., Shuvalov, V. A., Semenov, A. Y., and Nadtochenko, V. A. (2020) Visible and near infrared absorption spectrum of the excited singlet state of chlorophyll *a*, *High Energy Chem.*, **54**, 145-147, doi: 10.1134/S0018143920020058.
41. Cherepanov, D. A., Petrova, A. A., Mamedov, M. D., Vishnevskaya, A. I., Gostev, F. E., Shelaev, I. V., Aybush, A. V., and Nadtochenko, V. A. (2022) Comparative absorption dynamics of the singlet excited states of chlorophylls *a* and *d*, *Biochem.*, **87**, 1179-1186, doi: 10.1134/S000629792210011X.
42. Davydov, A. S. (1962) *The Theory Of Molecular Excitons*, McGraw-Hill, New York, NY.
43. Kasha, M., Rawls, H. R., and El-Bayoumi, M. A. (1965) The exciton model in molecular spectroscopy, *Pure Appl. Chem.*, **11**, 371-392, doi: 10.1351/pac196511030371.
44. Scholes, G. D., and Ghiggino, K. P. (1994) Rate expressions for excitation transfer I. Radiationless transition theory perspective, *J. Chem. Phys.*, **101**, 1251-1261, doi: 10.1063/1.467817.
45. Renger, T., and Marcus, R. A. (2002) On the relation of protein dynamics and exciton relaxation in pigment-protein complexes: an estimation of the spectral density and a theory for the calculation of optical spectra, *J. Chem. Phys.*, **116**, 9997-10019, doi: 10.1063/1.1470200.
46. Pieper, J., Rätsep, M., Trostmann, I., Schmitt, F. J., Theiss, C., Paulsen, H., Eichler, H. J., Freiberg, A., and Renger, G. (2011) Excitonic energy level structure and pigment-protein interactions in the recombinant water-soluble chlorophyll protein. II. Spectral hole-burning experiments, *J. Phys. Chem. B*, **115**, 4053-4065, doi: 10.1021/jp111457t.
47. Kell, A., Bednarczyk, D., Acharya, K., Chen, J., Noy, D., and Jankowiak, R. (2016) New insight into the water-soluble chlorophyll-binding protein from *Lepidium virginicum*, *Photochem. Photobiol.*, **92**, 428-435, doi: 10.1111/php.12581.
48. Adolphs, J., Berrer, M., and Renger, T. (2016) Hole-burning spectroscopy on excitonically coupled pigments in proteins: theory meets experiment, *J. Am. Chem. Soc.*, **138**, 2993-3001, doi: 10.1021/jacs.5b08246.
49. Gillie, J. K., Lyle, P. A., Small, G. J., and Golbeck, J. H. (1989) Spectral hole burning of the primary electron donor state of Photosystem I, *Photosynth. Res.*, **22**, 233-246, doi: 10.1007/BF00048302.
50. Pieper, J., Voigt, J., and Small, G. J. (1999) Chlorophyll a Franck–Condon factors and excitation energy transfer, *J. Phys. Chem. B*, **103**, 2321-2322, doi: 10.1021/jp984460e.
51. Peternian, E. J. G., Pullerits, T., van Grondelle, R., and van Amerongen, H. (1997) Electron-phonon coupling and vibronic fine structure of light-harvesting complex II of green plants: temperature dependent absorption and high-resolution fluorescence spectroscopy, *J. Phys. Chem. B*, **101**, 4448-4457, doi: 10.1021/jp962338e.
52. Förster, T. (1948) Intermolecular energy migration and fluorescence [in German], *Ann. Phys.*, **437**, 55-75, doi: 10.1002/andp.19484370105.
53. Cherepanov, D. A., Shelaev, I. V., Gostev, F. E., Aybush, A. V., Mamedov, M. D., Shuvalov, V. A., Semenov, A. Y., and Nadtochenko, V. A. (2020) Generation of ion-radical chlorophyll states in the light-harvesting antenna and the reaction center of cyanobacterial photosystem I, *Photosynth. Res.*, **146**, 55-73, doi: 10.1007/s11120-020-00731-0.
54. Cherepanov, D. A., Shelaev, I. V., Gostev, F. E., Aybush, A. V., Mamedov, M. D., Shen, G., Nadtochenko, V. A., Bryant, D. A., Semenov, A. Y., and Golbeck, J. H. (2020) Evidence that chlorophyll f functions solely as an antenna pigment in far-red-light photosystem I from *Fischerella thermalis* PCC 7521, *Biochim. Biophys. Acta Bioenerg.*, **1861**, 148184, doi: 10.1016/j.bbabio.2020.148184.
55. Shelaev, I. V., Gostev, F. E., Mamedov, M. D., Sarkisov, O. M., Nadtochenko, V. A., Shuvalov, V. A., and Semenov, A. Y. (2010) Femtosecond primary charge separation in *Synechocystis* sp. PCC 6803 photosystem I, *Biochim. Biophys. Acta Bioenerg.*, **1797**, 1410-1420, doi: 10.1016/j.bbabio.2010.02.026.

56. Van Stokkum, I. H. M., Müller, M. G., Weißenborn, J., Weigand, S., Snellenburg, J. J., and Holzwarth, A. R. (2023) Energy transfer and trapping in photosystem I with and without chlorophyll-*f*, *IScience*, **26**, 107650, doi: 10.1016/J.ISCI.2023.107650.
57. Pålsson, L.-O. O., Flemming, C., Gobets, B., van Grondelle, R., Dekker, J. P., and Schlodder, E. (1998) Energy transfer and charge separation in photosystem I: P700 oxidation upon selective excitation of the long-wavelength antenna chlorophylls of *Synechococcus elongatus*, *Biophys. J.*, **74**, 2611-2622, doi: 10.1016/S0006-3495(98)77967-6.
58. Gobets, B., Kennis, J. T. M., Ihalainen, J. A., Brazzoli, M., Croce, R., Stokkum, I. H. M. van, Bassi, R., Dekker, J. P., van Amerongen, H., Fleming, G. R., and van Grondelle, R. (2001) Excitation energy transfer in dimeric light harvesting complex I: a combined streak-camera/fluorescence upconversion study, *J. Phys. Chem. B*, **105**, 10132-10139, doi: 10.1021/jp011901c.
59. Riley, K. J., Reinot, T., Jankowiak, R., Fromme, P., and Zazubovich, V. (2007) Red antenna states of photosystem I from cyanobacteria *Synechocystis* PCC 6803 and *Thermosynechococcus elongatus*: single-complex spectroscopy and spectral hole-burning study, *J. Phys. Chem. B*, **111**, 286-292, doi: 10.1021/jp062664m.
60. Gisriel, C., Shen, G., Kurashov, V., Ho, M. Y., Zhang, S., Williams, D., Golbeck, J. H., Fromme, P., and Bryant, D. A. (2020) The structure of Photosystem I acclimated to far-red light illuminates an ecologically important acclimation process in photosynthesis, *Sci. Adv.*, **6**, eaay6415, doi: 10.1126/sciadv.aay6415.
61. Young, R. M., and Wasielewski, M. R. (2020) Mixed electronic states in molecular dimers: Connecting singlet fission, excimer formation, and symmetry-breaking charge transfer, *Acc. Chem. Res.*, **53**, 1957-1968, doi: 10.1021/acs.accounts.0c00397.
62. Casanova, D. (2018) Theoretical modeling of singlet fission, *Chem. Rev.*, **118**, 7164-7207, doi: 10.1021/acs.chemrev.7b00601.
63. Petrova, A. A., Casazza, A. P., Shelaev, I. V., Gostev, F. E., Aybush, A. V., Nadtochenko, V. A., Semenov, A. Y., Santabarbara, S., and Cherepanov, D. A. (2023) Role of pheophytin a in the primary charge separation of photosystem I from *Acaryochloris marina*: femtosecond optical studies of excitation energy and electron transfer reactions, *Biochim. Biophys. Acta Bioenerg.*, **1864**, 148984, doi: 10.1016/j.bbabio.2023.148984.
64. Akhtar, P., and Lambrev, P. H. (2020) On the spectral properties and excitation dynamics of long-wavelength chlorophylls in higher-plant photosystem I, *Biochim. Biophys. Acta Bioenerg.*, **1861**, 148274, doi: 10.1016/J.BBABIO.2020.148274.
65. Karapetyan, N. V., Bolychevtseva, Y. V., Yurina, N. P., Terekhova, I. V., Shubin, V. V., and Brecht, M. (2014) Long-wavelength chlorophylls in photosystem I of cyanobacteria: origin, localization, and functions, *Biochemistry (Moscow)*, **79**, 213-220, doi: 10.1134/S0006297914030067.